Interactions of CCl_4 with Thin D_2O Amorphous Ice Films, Part I: A Nanoscale Probe of Ice Morphology

V. Sadtchenko, K. Knutsen, Clayton F. Giese, and W. Ronald Gentry*

Department of Chemistry, University of Minnesota, 207 Pleasant Street SE, Minneapolis, Minnesota 55455

Received: July 27, 1999; In Final Form: December 15, 1999

High sensitivity temperature-programmed desorption mass spectrometry (TPDMS) was used in order to investigate the adsorption of carbon tetrachloride on thin (∼500 ML) amorphous D_2O ice films at 95 K. The TPDMS experiments demonstrate that the desorption kinetics of CCl_4 are extremely sensitive to the ice morphology. At submonolayer coverages, the adsorption of CCl_4 on ice films prepared by vapor deposition at 130 K results in TPD spectra which consist of a single desorption feature α-CCl_4 at 133−140 K. The TPD spectrum of CCl_4 from ice films vapor-deposited at 95 K, however, consists of three desorption peaks labeled σ-, δ-, and ϵ-CCl_4 at 145, 180, and 190 K, respectively. We attribute the observed differences in the TPD spectra of CCl_4 from the two types of ice to differences in the microstructure of the ice surface. D_2O vapor deposition at 95 K apparently results in the formation of microporous amorphous ice, while deposition at 130 K results in the formation of pore-free, solid ice. Analysis of the TPD spectra demonstrates that CCl_4 adsorption on ice prepared at 130 K results in the formation of metastable, two-dimensional islands. CCl_4 adsorption on ice prepared at 95 K, however, proceeds through formation of three-dimensional clusters in the pores of microscopically rough ice. At very low coverages, small CCl_4 clusters are trapped at the ice surface during TPD. Trapped CCl_4 evolves into the gas phase at two different temperatures giving rise to δ- and ϵ-CCl_4 desorption states. The dependence of δ- and ϵ-CCl_4 yields on the temperature of ice film deposition indicates that two structurally different forms of ice coexist at temperatures between 95 and 130 K.

Introduction

The physics and chemistry of ice surfaces has attracted considerable research interest in such diverse areas of science as environmental, interstellar, and biological chemistry. The importance of the ozone loss problem, for example, has stimulated intense laboratory studies of stratospherically relevant heterogeneous reactions on the surface of ice and acid hydrate particles.[1−12] The molecular structure of ice surfaces is also a matter of fundamental interest. Ice is often regarded as a model system for the study of the surface properties of molecular solids due to the availability of extensive experimental and theoretical data on intermolecular interactions in liquid water and ice.

Depending on pressure and temperature, ice can exist in a number of structurally different forms. At low pressures (<0.2 kbar), there are two known crystalline states: a diamond cubic form (I_c) and a hexagonal phase (I_h). When grown in a vacuum by a vapor deposition on a cold substrate, cubic and hexagonal crystalline ice are formed at substrate temperatures above 133 and 153 K, respectively.[13]

The deposition of water vapor at substrate temperatures below 130 K results in the formation of low-density amorphous ice (ρ < 0.93 g/cm^3).[13,14] Various experimental techniques have been applied in order to study the molecular structures of thin amorphous H_2O and D_2O ice films. Studies of structure, morphology, surface area, density, and vapor pressure of amorphous ice films indicate a large range of physical properties, depending on the preparation conditions. Measurements of the surface area of the amorphous ice result in values ranging from a few m^2/g to several hundreds of m^2/g.[15−18] Studies of the refractive index of vapor-deposited amorphous ice films demonstrated that the density of the amorphous ice changes with temperature and the rate of ice deposition. At temperatures above 120 K, the ice films had a density $\rho = 0.93$ g cm^{-3}. Densities as low as 0.65 g cm^{-3}, however, were found at lower temperatures.[19]

Recently, grazing angle FTIR spectroscopy was used to monitor the relative abundance of incompletely coordinated water molecules in the bulk of the amorphous ice formed by vapor deposition at different temperatures and pressures. Similar to the ice density, the dangling bond (free OH stretch) signal associated with or two- or three-coordinated water molecules was found to vary significantly with the temperature and pressure of ice deposition. The largest dangling bond signal was observed at 94 K under conditions of fast ice growth, while the smallest signal was observed at 120 K under conditions of slow growth.[20]

These results are often interpreted as evidence of the high porosity of amorphous ice. Microporous amorphous ice forms at low temperatures (<120 K) when diffusion of water molecules along the ice surface is slow. At high rates of ice deposition, water molecules have insufficient time to rearrange before being buried by subsequent adlayers. This results in formation of a microporous ice structure with a large number of incompletely coordinated water molecules at the pore surfaces. Extensive experimental and theoretical study by Devlin, Buch et al. suggests that amorphous ice vapor deposited at substrate temperatures below 90 K is always microporous.[21−28]

Recently, Kay et. al. reported the results of surface area measurements of thin ice films prepared by various techniques.[29] According to these researchers, pore-free H_2O ice films can be

* Corresponding author.

10.1021/jp9926185 CCC: $19.00
Published on Web 02/29/2000

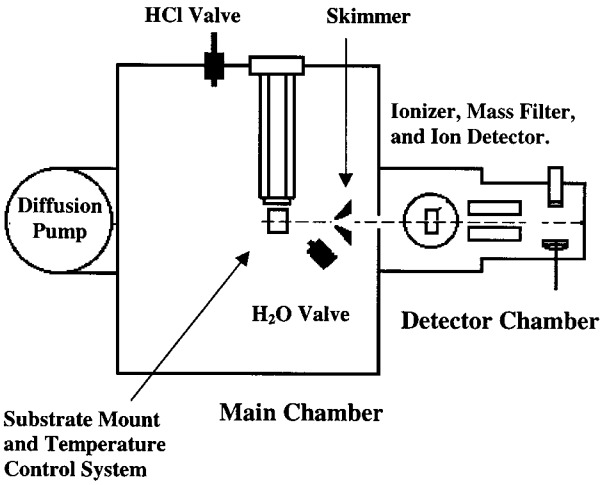

Figure 1. Schematic representation of the experimental apparatus. Features are not shown to scale.

grown at temperatures as low as 50 K if a well-collimated H_2O-vapor beam at normal incidence is used for deposition. This result, however, is rather an exception to the general trend, due to the very special ice deposition technique used. Indeed, the experiments of Kay et al., also show that highly porous ice films result from deposition at low temperatures from the ambient vapor.[29]

At deposition temperatures above 125−130 K and low deposition rates (typically <0.5 ML s^{-1}), the resulting amorphous ice structure, however, is expected to be free of micropores.[19,20] The distinction can therefore be made between solid amorphous (SA) and microporous amorphous (MA) ice. (Solid amorphous ice should not be confused with high-density amorphous ice, which forms at pressures above 2 kBar.)

Development of new methods for investigation into the surface properties of molecular solids has recently become the focus of our research. The variability of amorphous ice microstructure makes this type of ice an excellent model system for study. In our experiments, we employ high sensitivity TPDMS in order to investigate adsorption of weakly interacting molecules on the surface of thin (∼500 ML) amorphous D_2O ice films prepared in a vacuum by D_2O vapor condensation on a cold substrate. Here, we report the results of kinetic measurements of CCl_4 desorption from amorphous D_2O ice films prepared under varying conditions. Carbon tetrachloride was chosen for these experiments because ice and CCl_4 are immiscible. Two principal goals were pursued in these experiments. First, the influence of ice surface morphology on the adsorption states and desorption pathways of CCl_4 was investigated. Second, using CCl_4 desorption as a probe of surface morphology, we attempted to gain insights into the microstructure of the different forms of amorphous D_2O ice. Our TPDMS experiments demonstrate that at submonolayer coverages CCl_4 desorption from D_2O ice films strongly depends on the ice preparation conditions and, thus, provides valuable information on ice surface morphology.

Experimental Section

Apparatus. A schematic diagram of the apparatus is shown in Figure 1. The instrument modified for these experiments was previously used for crossed molecular beam and photodissociation studies.[30] The experiments were conducted in a vacuum chamber pumped with a 10000 L/s Varian HS-20 oil diffusion pump. D_2O ice films were vapor-deposited on a small (5 mm diameter, 0.5 mm thick) platinum substrate. The substrate was in thermal contact with a liquid nitrogen cooled reservoir. A tungsten filament was positioned behind the substrate. Between 95 and 800 K, the substrate temperature was varied through balancing of radiative heating against thermal conductance. Heating/cooling rates in excess of 100 K/s were achieved with this experimental arrangement.

The distance to the substrate and the shape of the filament were adjusted in order to minimize the temperature gradient across the substrate. During preliminary experiments, the temperature of the substrate was simultaneously monitored with several miniature thermocouple junctions spot-welded at various points across the surface of the Pt substrate. These measurements demonstrated that during TPDMS experiments the temperature difference across the substrate did not exceed 1 K. Substrate temperature was monitored regularly with a single copper−constantan thermocouple junction spot-welded to the edge of the substrate.

The substrate was positioned on the line of sight of a differentially pumped quadrupole mass spectrometer. This part of the experimental apparatus has been described in detail elsewhere.[30] The mass spectrometer employed a custom-built electron impact ionizer and a Daly type ion counter.[31] The detector chamber consisted of two differentially pumped regions. The outer region, which contained a quadrupole mass filter, ion optics, and the ion detector, was maintained at $\sim 5 \times 10^{-9}$ Torr. The inner region, which contained the electron impact ionizer, was maintained at $\sim 5 \times 10^{-10}$ Torr. A small skimmer, placed between the substrate and the detector, allowed only desorption products generated at the substrate to enter the detector and blocked any direct path from parts of the substrate mount, which might have experienced heating during TPDMS experiments.

The vacuum arrangements employed in our experiments have several apparent advantages. First, due to a very high pumping speed, we were able to conduct direct rate measurements of desorption kinetics. Preliminary TPDMS experiments demonstrated that the signal due to direct desorption flux from the substrate surface was at least 2 orders of magnitude higher than the signal due to the increase of partial pressure of desorption products in the main chamber. Second, we were able to conduct TPDMS in experiments with relatively thick (500 ML) D_2O ice films. Third, differential pumping of the detector ensured a high signal-to-noise ratio. Though relatively high partial D_2O and CCl_4 pressures ($>10^{-6}$ Torr) were typically maintained inside the main chamber during the film deposition, virtually no detectable contamination of the ionizer chamber with D_2O or CCl_4 was observed.

To avoid the mixing of the adsorbates prior to deposition, D_2O and CCl_4 were admitted into the main chamber via completely independent stainless steel lines. A direct-flow solenoid valve (General Valve) positioned at about 10 cm from the Pt substrate was used as an effusive source for D_2O deposition. The small diameter of the Pt substrate ensured the relative uniformity of the D_2O deposition flux across the substrate. Since the D_2O vapor source was uncollimated, the D_2O vapor flux at the substrate surface was characterized by a large variation in the incidence angle and energy of the impinging D_2O molecules. Such a regime of ice film deposition is similar to the condensation from ambient vapor. D_2O deposition flux was controlled via adjustment of the stagnation pressure of the effusive source. The performance of the D_2O doser was characterized using a fast-ionization gauge (FIG) positioned 15 cm from the aperture of the source.[30] These tests demonstrated that a very high stability of the D_2O flux was achieved for the wide range of stagnation pressures. The short

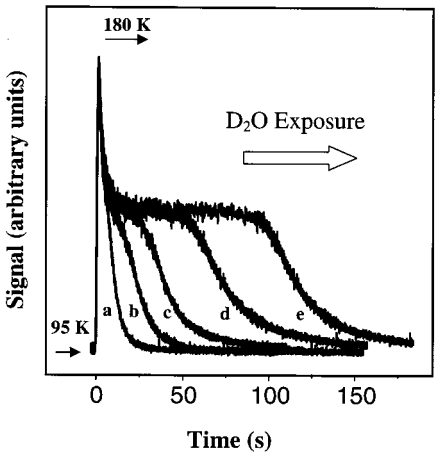

Figure 2. Isothermal spectra of D_2O ice films vapor-deposited on Pt substrate at 95 K. The deposition time was 10 (a), 17 (b), 30 (c), 50 (d), and 80 s (e). D_2O flux was approximately 2 ML s^{-1}.

actuation time of the solenoid valve (2 ms) allowed a fast cutoff of the D_2O deposition flux upon the end of the deposition process. CCl_4 was deposited on the substrate by pressurizing the main chamber with CCl_4 vapor.

Liquid D_2O (Isotope Laboratories) and carbon chloride (Spectrum Chemicals, ACS grade) were degassed before use each day. Depending on the type of experiment (isothermal desorption or temperature-programmed desorption), the D_2O signal was monitored at *m*/*e* 22 ($D_2{}^{18}O^+$) or at *m*/*e* 20 ($D_2{}^{16}O^+$). CCl_4 was detected as *m*/*e* 117 ($C^{35}Cl_3{}^+$), the most abundant CCl_4 derived ion in the mass spectrometer. CCl_4 exposures were given in units of Torr s, the product of the time and the background pressure rise upon opening the CCl_4 doser.

A typical TPDMS experimental cycle began with cleaning of the substrate. Volatiles were removed from the substrate surface by heating of the substrate to 500 K for 20−50 s. The substrate was rapidly cooled to the desired temperature, and a D_2O ice film was deposited. After the ice film preparation and CCl_4 dosing, a TPDMS spectrum was obtained. This experimental cycle was repeated, varying D_2O or CCl_4 conditions as desired. All steps in an experimental cycle were controlled via PC computer with a multipurpose data acquisition board (National Instruments). Computer control of the film deposition process ensured high reproducibility of the results obtained in TPDMS experiments.

The vacuum conditions in our experiments raise concerns about ice surface contamination. We have determined, however, that the background gas condensation rate at the ice surface was less than 0.005 ML/s. The main "contaminant" was background H_2O. The typical time scale of the TPDMS experiments was short in comparison with the lifetime of the ice films.

Ice Film Characterization. Isothermal desorption studies were conducted in order to characterize vapor-deposited D_2O ice films. The films, initially maintained at 95 K, were rapidly heated; the heating rate during the temperature jump was approximately 80 K/s. Isothermal desorption (ID) spectra of D_2O ice films obtained at several D_2O exposures are shown in Figure 2. All films were grown at 95 K.

At very low D_2O exposures, the ID spectrum is characterized by fast monotonic signal decay. At higher D_2O exposures, however, three regions of distinctly different kinetics are observed. The desorption rate exhibits an initial rapid increase due to ramping the temperature from 95 to 180 K. At 180 K, the desorption rate decreases rapidly to a value approximately half the initial rate. The rapid decline of the desorption rate is followed by a region of apparently zero-order desorption kinetics. The desorption kinetics change again when a significant fraction of the ice film has evolved into the gas phase and a monotonic decline in the desorption rate is observed.

The ID spectra shown in Figure 2 are similar to the ID spectra previously reported for sublimation of thin (10−100 ML) amorphous ice films deposited on clean platinum and graphite substrates.[32,33] The high initial sublimation rate of amorphous ice indicates that crystallization is not complete during the temperature jump. Thus, the desorption rate decreases as the amorphous ice undergoes crystallization in parallel with sublimation. The zero-order desorption kinetics consistent with sublimation of a smooth, solid, and pore-free ice film is observed once ice crystallization is complete. Any kind of ice surface roughening or smoothing during sublimation is likely to change the effective surface area of the film, and thus, must result in nonzero order desorption kinetics. Such a change in sublimation kinetics apparently takes place when the ice films reach some critical thickness. The breaking of a very thin film into 3D-islands or droplets must occur at this point.[32,33] Zero-order sublimation kinetics, observed in isothermal desorption measurements, also indicate that the temperature lag between the platinum substrate and the ice surface is small. If the temperature lag were significant, the surface temperature of the sublimating ice film would depend on the film thickness and nonzero-order sublimation kinetics would be observed.

Isothermal measurements of the D_2O sublimation rate at known temperatures were used in order to estimate the film thickness and the deposition flux. The zero-order sublimation rate at a known temperature can be calculated using the following equation:

$$R(T) = \nu_0 \exp\left(\frac{-E_{D_2O}}{RT}\right) \quad (1)$$

where ν_0 is the zero-order desorption factor (4.0×10^{30} molecules cm^{-2} s^{-1}),[34,45] and E_{D_2O} is the desorption activation energy (53.2 kJ mol^{-1}).[34,35] Assuming that a single monolayer of a crystalline ice film contains about 10^{15} cm^{-2} D_2O molecules,[35] the thickness of the D_2O ice films can be determined in monolayer equivalents by integration of the ID or TPD spectra of the films over desorption time. Once the thickness of an ice film is calculated, it is possible to determine the D_2O vapor flux at the surface of the substrate during deposition. Assuming that the sticking probability for water molecules at 95 K is unity, the D_2O flux near the substrate surface in ML s^{-1} units is defined as the ratio of the ice film thickness to the deposition time. These procedures apparently provide only a rough estimate of film thickness. The error in the D_2O deposition flux and the film thickness arises from uncertainties in the desorption activation energy (E_{D_2O}), pre-exponential factor (ν_0), and the desorption temperature measurements. These errors, however, have a systematic character and do not affect relative thickness or deposition flux measurements.

The zero-order desorption kinetics observed after crystallization of the amorphous ice implies that, even prior to crystallization, amorphous D_2O ice films completely cover the Pt substrate. Given that D_2O mobility is low at 95 K, it is hard to imagine the formation of separated clusters of amorphous ice.[19,20] It also seems unlikely that, even if formed, large clusters of amorphous ice would produce a smooth solid ice film upon crystallization. Nevertheless, to further validate this conclusion, we have investigated isothermal desorption of a multilayer CCl_4 film covered with ~500 ML of amorphous ice.

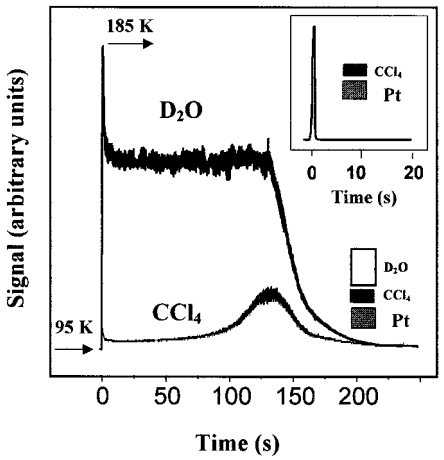

Figure 3. ID spectrum of CCl_4 covered with a ~500 ML thick D_2O ice film. CCl_4 ID spectrum in the absence of the D_2O adlayer and D_2O ID spectrum are shown for comparison.

ID spectra of CCl_4 and D_2O obtained upon heating of such a film to 185 K are shown in Figure 3. The initial heating rate was about 100 K/s. The ID spectrum of a multilayer CCl_4 film from the Pt substrate is shown for comparison. In the absence of the D_2O layer, desorption of the carbon tetrachloride is exceedingly fast at 185 K. The entire CCl_4 film evolves into the gas phase in less than 2 s. CCl_4 desorption, however, is drastically inhibited when ~500 ML of amorphous D_2O ice is deposited on top of the CCl_4 film. Apparently, more than 95% of the carbon tetrachloride is retained until most of the overlaying D_2O ice film sublimes. These measurements clearly demonstrate that amorphous ice, though microporous, is free of connected pathways that traverse entire bulk of the ice film. It also follows from these experiments that structural changes during phase transitions from amorphous to crystalline ice do not lead to formation of large ruptures in the bulk of the 500 ML thick D_2O ice films. The last conclusion does not contradict results obtained by Smith et al.[36] They have observed an abrupt desorption of carbon tetrachloride in the TPD experiments with D_2O/CCl_4 films, driven by crystallization of the overlaying amorphous ice. The D_2O ice films in our experiments are significantly thicker compared to the ice films studied by Smith et al. (<260 ML). We were able to reproduce the results of these researchers in experiments with much thinner (<100 ML) ice films.

Isothermal desorption experiments with D_2O ice films vapor-deposited at 95 K were also repeated with the ice films grown at higher temperatures. No significant changes were observed in the ID spectra of pure D_2O ice films grown at 130 K compared to the spectra of the ice films grown at 95 K. Experiments with 500 ML thick D_2O films grown on the top of multilayer CCl_4 films at 125 K resulted in the CCl_4 and D_2O spectra which were similar to the spectra shown in Figure 3. At 185 K, the desorption of carbon tetrachloride was effectively blocked until most of the overlaying ice film had sublimed.

Common Experimental and Procedures. To successfully disentangle different factors which determine ice morphology and the CCl_4 desorption pathways, some of the conditions had to be identical in each experiment. In all experiments reported in this work, the thickness of the ice film was the same and equal to approximately 500 ML. During the growth of the ice films, the D_2O deposition flux was always 0.5 ML s^{-1}. In all experiments, CCl_4 was deposited at 95 K. The partial pressure of carbon tetrachloride inside the main chamber during CCl_4 deposition was always 1×10^{-6} Torr, as measured with an ion gauge. In all experiments, a 15 s delay was allowed after D_2O ice deposition before the experiment would proceed with the CCl_4 deposition. This short delay ensured the cooling of the Pt substrate to 95 K whenever D_2O deposition took place at higher temperatures. A 1 s delay was also allowed before a TPDMS cycle in order to minimize the background signal. The 500 ML thick solid amorphous (SA) ice films were prepared by D_2O vapor deposition at 130 K. Microporous amorphous (MA) D_2O films of the same thickness were deposited at 95 K.

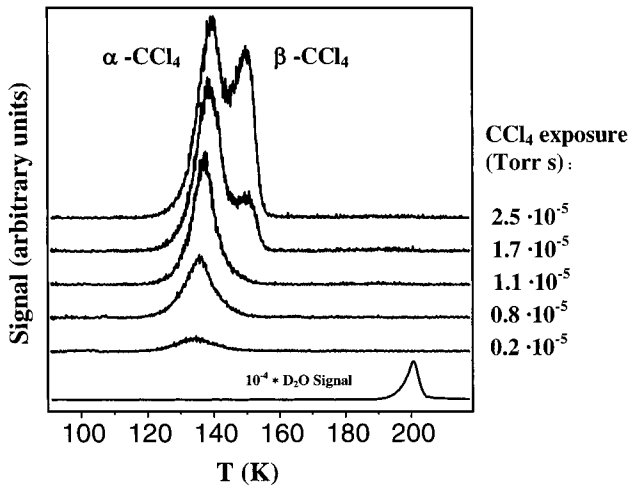

Figure 4. TPD spectra of CCl_4 from solid amorphous ice at the low CCl_4 exposures.

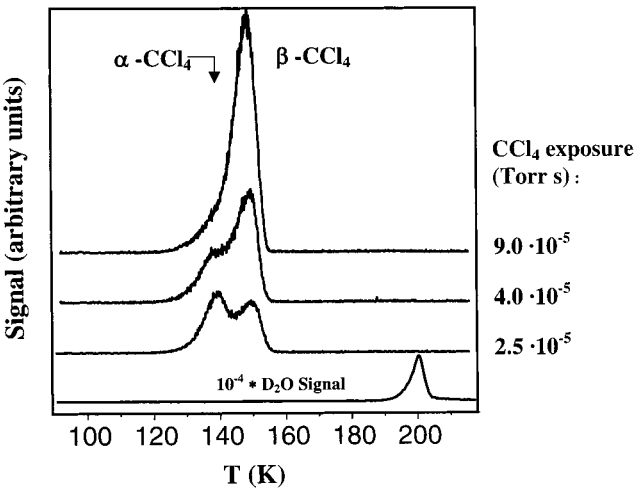

Figure 5. TPD spectra of CCl_4 from solid amorphous ice at high CCl_4 exposures.

Results and Discussion

I. Adsorption of CCl_4 on the Surface of Solid Amorphous D_2O Ice. *TPD Spectra.* The results of the desorption experiments represented here are in general agreement with the results of similar studies conducted by Blanchard and Roberts.[37] Figures 4 and 5 show TPD spectra of CCl_4 obtained for CCl_4 exposures in the range from 2×10^{-6} to 10^{-4} Torr s. At very low exposures, a single peak, designated as α-CCl_4, is observed at 133 K. The α-CCl_4 yield and desorption temperature gradually increase with exposure until a second peak, designated as β-CCl_4, appears in the TPD spectra at ~150 K. An increase in the CCl_4 exposure above 10^{-5} Torr s leads to a rapid saturation of the α-CCl_4 feature. At exposures above 2.5×10^{-5} Torr s, the α-CCl_4 yield gradually declines while the α-CCl_4 yield

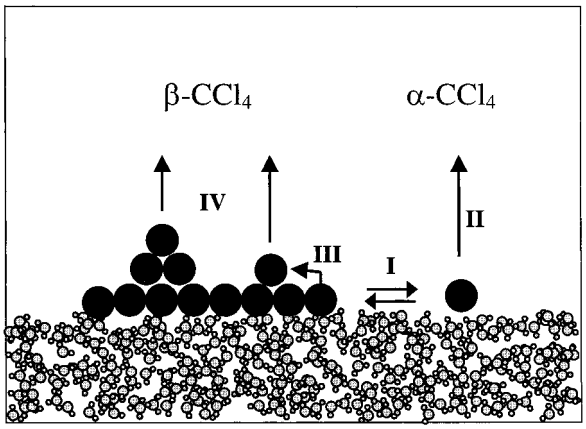

Figure 6. Desorption pathways of CCl_4 from solid amorphous ice: (I) reversible dissociation from the island edges; (II) free CCl_4 monomer desorption; (III) three-dimensional nucleation; (IV) condensed phase sublimation.

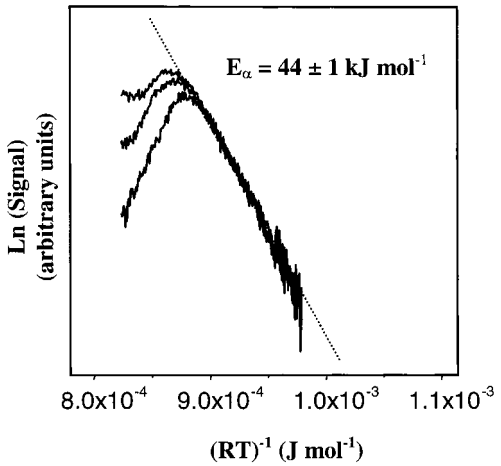

Figure 7. Arrhenius plot of the α-CCl_4 peaks. CCl_4 exposures were from 1.1 to 2.5 × 10^{-5} Torr s.

continues to increase. At a CCl_4 exposure of about 10^{-4} Torr s, the α-CCl_4 peak disappears completely from the TPD spectra. Further increase in CCl_4 exposure results in TPD spectra that consist solely of the β-CCl_4 peak. Above 10^{-4} Torr s, the β-CCl_4 desorption peak is consistent with the sublimation of a multilayer CCl_4 film. Arrhenius analysis of the TPD spectra in cases of high CCl_4 exposures gives an apparent activation energy of 37 ± 1 kJ mol^{-1} for β-CCl_4 desorption, which is in good agreement with the literature value of the apparent activation energy for sublimation of a multilayer CCl_4 phase (38 kJ mol^{-1}).[37,38]

In addition to coverage dependence, we have briefly investigated the dependence of the TPD spectra on heating rate. Similar to Blanchard and Roberts, we have observed a significant increase in the α-CCl_4 and a proportional decline in the β-CCl_4 yield at higher heating rates.

State of the CCl_4 Adsorbate and the Desorption Pathways. The observed TPD spectra are consistent with formation of CCl_4 islands on the surface of solid amorphous D_2O ice. The CCl_4 desorption pathways are summarized in Figure 6. According to Blanchard and Roberts, metastable, two-dimensional CCl_4 islands are formed on the surface of ice at low CCl_4 exposures.[37] Desorption of these islands proceeds through a two-step mechanism. First, a reversible dissociation of CCl_4 molecules from an island edge takes place (I). Dissociation from the island edge is followed by desorption of free CCl_4 monomers directly from the D_2O ice surface (II). This desorption channel gives rise to the α-CCl_4 peak in the TPD spectra. Formation of three-dimensional CCl_4 islands is also possible as a result of nucleation barrier crossing by CCl_4 molecules adsorbed at the island edges (III). Desorption of the multilayer CCl_4 phase results in a β-CCl_4 TPD peak (IV).

Such an assignment of α- and β- CCl_4 desorption features explains the observed TPD spectrum dependence on CCl_4 exposure. The increase in β-CCl_4 yield at low heating rates implies that the barrier to CCl_4 molecule migration on the top of the 2D islands is higher than the barrier to dissociation from the island edge. The low rate of CCl_4 monomer recapture at island edges and abundance of sites for CCl_4 monomer desorption results in predominant α-CCl_4 desorption at low CCl_4 coverages.

As islands grow, the number of sites available for free CCl_4 monomer desorption decrease. CCl_4 monomer recapture as well as the adsorption of CCl_4 molecules on top of the 2D islands becomes more likely. As a result, the rapid decline in α-CCl_4 yield and the increase in β-CCl_4 yield is observed at higher CCl_4 exposures. The disappearance of the α-CCl_4 peak from TPD spectra at very high exposures is consistent with the coalescence of CCl_4 islands and formation of the multilayer CCl_4 film that covers the entire ice surface. TPD spectra of CCl_4 obtained at exposures above 10^{-4} Torr represent sublimation of multilayer CCl_4 films.

At CCl_4 exposures below 2.5 × 10^{-5} Torr s, the leading edges of the α-CCl_4 peaks are superimposable, which implies zero-order desorption kinetics. Several theoretical treatments have been applied to the system represented in Figure 4.[39] Depending on the coverage and temperature, these theories predict zero-order kinetics for desorption of island ensembles. Zero-order kinetics have also been observed experimentally for desorption of Xenon islands from graphite substrates.[40] Arrhenius plots of the TPD spectra obtained at three CCl_4 exposures are shown in Figure 7. A linear dependence of the logarithm of the desorption rate on inverse temperature is evident for the leading edges of α-CCl_4 desorption peaks. From the slope of the Arrhenius plot, the apparent activation energy for α-CCl_4 desorption (E_α) was determined. The obtained value of $E_\alpha = 44 \pm 1$ kcal mol^{-1} is in good agreement with the value reported by Blanchard and Roberts (47 ± 3 kJ mol^{-1}).[37]

The activation energy for α-CCl_4 desorption is significantly higher than that for sublimation of the condensed CCl_4 phase, which is about 38 kJ mol^{-1} [34]. The fact that α-CCl_4 desorption occurs at much lower temperatures as compared to the desorption temperature of the multilayer phase implies that α-CCl_4 desorption is characterized by a higher frequency factor. The differences in frequency factors for α-CCl_4 and β-CCl_4 desorption can be explained by the differences in entropy of CCl_4 at the edge of a 2D island and in the multilayer phase.[37]

Summary. Our TPD experiments demonstrate that the state of the CCl_4 adsorbate and the desorption pathways on SA D_2O ice are essentially the same as on H_2O amorphous ice. In cases of low exposures, CCl_4 exists at the ice surface in the form of two-dimensional islands (Figures 8 and 9). The desorption of CCl_4 islands proceeds through dissociation from the island edge followed by free CCl_4 monomer desorption from the ice surface. The apparent activation energy for this desorption channel is 44 ± 1 kJ mol^{-1}.

II. Adsorption of CCl_4 on the Surface of Microporous Amorphous D_2O Ice. *TPD Spectra.* The TPD spectra of CCl_4 from MA ice obtained at various CCl_4 exposures are shown in Figures 8−10. At CCl_4 exposures below 5 × 10^{-6} Torr s, two desorption features are observed in the TPD spectra: a narrow peak at 180 K, designated as δ-CCl_4, and a shoulder at 190 K,

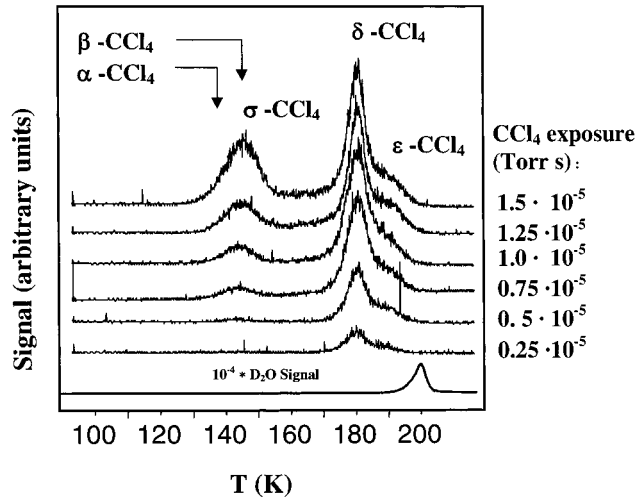

Figure 8. TPD spectra of CCl_4 from microporous amorphous ice at low CCl_4 exposures.

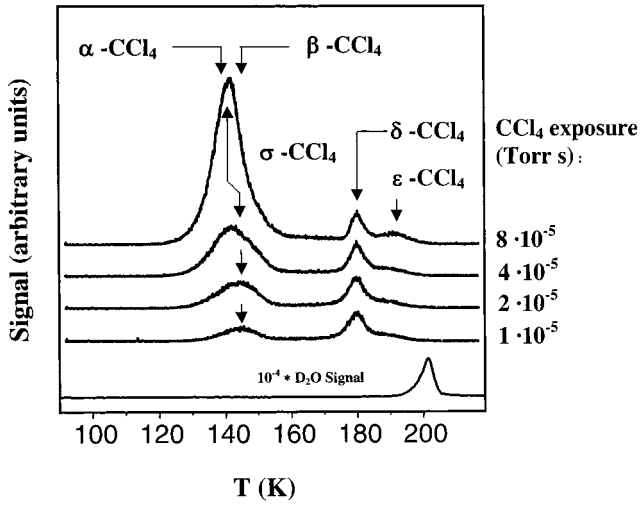

Figure 9. TPD spectra of CCl_4 from microporous amorphous ice at high CCl_4 exposures.

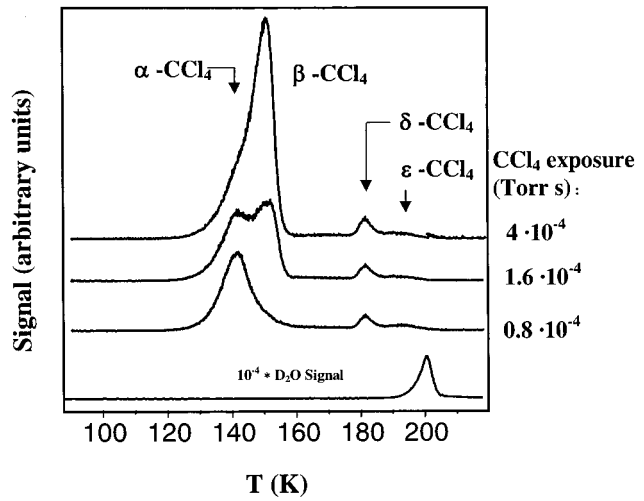

Figure 10. TPD spectra of CCl_4 from microporous amorphous ice at very high CCl_4 exposures.

designated as ϵ-CCl_4. Apparently, the variation in deposition conditions of the ice films results in significant changes in the CCl_4 TPD spectra. Note that at similar CCl_4 exposures the TPD spectra of CCl_4 from SA ice consist of a single peak at 133 K (Figure 4).

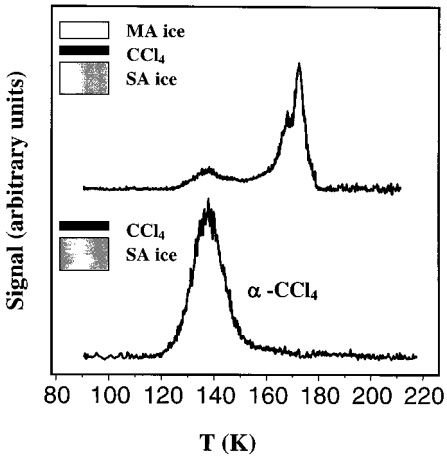

Figure 11. TPD spectra of $D_2O/CCl_4/D_2O$ sandwich film.

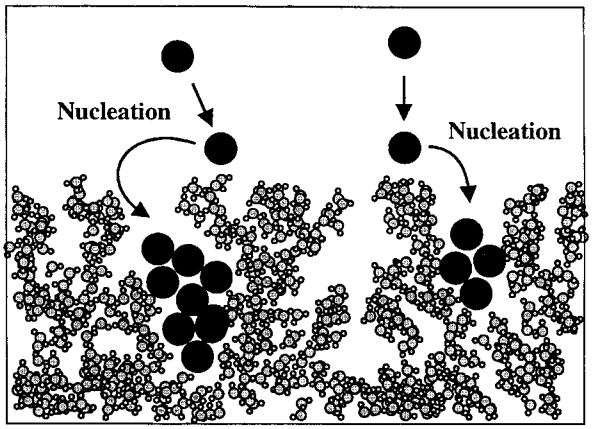

Figure 12. Microstructure of MA ice and its effect on the adsorption of carbon tetrachloride.

The increase in CCl_4 exposure from 7.5 to 15 $\times$ 10^{-6} Torr s leads to saturation in the δ- and ϵ-CCl_4 desorption features. Furthermore, at a CCl_4 exposure of 7.5 $\times$ 10^{-6} Torr s, another desorption feature designated as σ-CCl_4 appears in the TPD spectra at ~145 K. The σ-CCl_4 desorption feature exhibits a complex dependence on CCl_4 coverage. At CCl_4 exposures from 7.5 to 15 $\times$ 10^{-6} Torr s. The σ-CCl_4 peak grows and shifts slightly to higher temperatures. This behavior changes abruptly at exposures above 2 $\times$ 10^{-5} Torr s. The σ-CCl_4 peak broadens and shifts toward lower temperatures. The shift toward lower temperatures is complete when the σ-CCl_4 peak is located at ~140 K.

At CCl_4 exposures above 10^{-4} Torr s, the TPD spectra of CCl_4 from MA ice strongly resemble the TPD spectra of CCl_4 from SA ice; the σ-CCl_4 peak rapidly saturates, and a desorption feature, which is essentially identical to β-CCl_4, appears at ~150 K. Similar to the β-CCl_4 peak in the TPD spectra of CCl_4 from SA ice, this desorption feature does not saturate in the entire range of the experimental CCl_4 exposures. Furthermore, an increase in the CCl_4 exposure above 10^{-4} Torr s results in a gradual decline of the σ-CCl_4 yield. At exposures above 4 $\times$ 10^{-4} Torr s, the σ-CCl_4 peak disappears completely from the TPD spectra. An Arrhenius analysis of the TPD spectra in cases of very high CCl_4 exposure results in the apparent activation energy of 38 kJ mol^{-1}, consistent with sublimation of the multilayer CCl_4 film.[37,38]

Comparison of the CCl_4 TPD spectra from MA and SA ice indicates that the state of the CCl_4 adsorbate is different on the two types of ice surface at low CCl_4 coverage. The increase in desorption temperature by more than 40 K observed for carbon

tetrachloride on MA ice at low CCl_4 coverages cannot be explained by differences in the abilities of the two types of ice to form chemical bonds. The hydrophobic nature of CCl_4/D_2O interactions rules out the formation of strong chemical bonds between this particular molecule and either type of ice surface.[41] The δ-CCl_4 and ϵ-CCl_4 desorption features cannot be explained by interactions of carbon tetrachloride with the Pt substrate either. As we have determined, the TPD spectra of CCl_4 from a Pt substrate at low CCl_4 exposures consist of a single peak near 145 K. It should be noted, however, that the temperatures of δ-CCl_4 and ϵ-CCl_4 desorption are close to the temperatures of intense sublimation of the D_2O ice. We would like to argue, therefore, that the desorption features δ- and ϵ-CCl_4 appearing at 180−190 K in the TPD spectra of CCl_4 at exposures below 5×10^{-6} Torr s are derived from CCl_4 trapped in the near-surface region of the microporous D_2O ice.

The assignment of the δ- and ϵ-CCl_4 desorption features to desorption of CCl_4 trapped in the near-surface regions of the ice film is confirmed by desorption experiments with $D_2O/CCl_4/D_2O$ sandwich films. Figure 11 demonstrates the variation in TPD spectra of low coverage CCl_4 films deposited on SA ice and later exposed to D_2O flux at 95 K. The thickness of the SA ice film was about 500 ML, and CCl_4 exposure was 5×10^{-6} Torr s. The TPD spectrum of CCl_4 from solid D_2O ice at this exposure consists solely of an α-CCl_4 peak. The deposition sequence described above should result in formation of a porous amorphous D_2O layer with microporous ice at least partially covering and trapping the CCl_4 adsorbate. As expected, the deposition of a microporous amorphous ice layer on top of the CCl_4 film leads to significant hindrance of CCl_4 desorption. A desorption feature observed at 165−170 K in the TPD spectrum of the sandwich films is similar to δ- and ϵ-CCl_4 desorption peaks in the TPD spectra of CCl_4 from MA ice.

H_2, Ar, HCN, CH_3OH, and a number of other vapors and gases can easily be trapped in H_2O ice during co-deposition on a cold substrate.[42] The TPD spectra of such seeded films often include a few desorption features in the temperature range from 160 to 180 K. To our knowledge, however, trapping of adsorbates *at the surface* of thin amorphous D_2O or H_2O ice films has never been observed before, at least under the conditions present in our experiments.

State of CCl_4 Adsorbate and the Desorption Mechanisms. The complexities of CCl_4 desorption from MA ice are easily understood if the effect of the ice surface morphology on the state of the CCl_4 adsorbate is taken into consideration.

The ice deposition conditions present in our experiments ($T \approx 95$ K, D_2O deposition flux ≈ 0.5 ML s^{-1}) are consistent with the conditions of ballistic deposition.[19,20,43] The formation of pore-free, microscopically smooth ice is possible only if the surface diffusion rate at a particular temperature is sufficiently high so that a diffusing D_2O molecule can find a favorable adsorption site before it is covered by the next ice bilayer. Apparently, this is not the case when D_2O ice is grown at 95 K. The diffusion of D_2O molecules along the ice surface is expected to be extremely slow at this temperature.[19,20] Figure 12 represents the likely structure of MA ice and its effect on CCl_4 adsorption. The microstructure of the ice film, depicted in the Figure 12, is similar to structures resulting from computer simulations of multilayer adsorbates formed under conditions of ballistic deposition.[43] The crevices on the surface of microporous D_2O ice should provide the most energetically favorable sites for CCl_4 adsorption. Furthermore, the negative surface curvature in the ice pores is likely to result in lowering of the barrier to CCl_4 nucleation. We suggest that unlike the CCl_4 adsorption on the surface of SA ice, which results in the formation of two-dimensional CCl_4 islands, the adsorption of CCl_4 on the surface of microscopically rough MA D_2O ice must proceed through formation of three-dimensional CCl_4 clusters.

The assumption that CCl_4 adsorption on MA ice results in the formation of CCl_4 clusters in the ice micropores is essential for understanding of the CCl_4 TPD spectra obtained at any CCl_4 exposure. For the sake of convenience, let us introduce a parameter η defined as the ratio of the CCl_4 cluster size to the effective size of a micropore,

$$\eta = \frac{\langle N \rangle V_{CCl_4}}{\langle V_{pore} \rangle} \tag{2}$$

where $\langle V_{pore} \rangle$ is the average volume of the micropore, $\langle N \rangle$ is the average number of the CCl_4 molecule in the cluster, and V_{CCl_4} is the volume occupied by a single CCl_4 molecule. Three assumptions are necessary in order to explain the dependence of the TPD spectra on CCl_4 exposure. First, trapping of CCl_4 is possible only if the parameter η does not exceed some critical value $\eta_{cr} < 1$. Second, the collapse of the micropores containing large CCl_4 clusters ($\eta > \eta_{cr}$) is impeded until the size of the clusters is reduced during cluster evaporation in the course of TPD. Third, considering the large size of the CCl_4 molecule relative to D_2O, it is logical to assume that only a small fraction of pores on the ice surface can contain CCl_4 clusters. Furthermore, since the amplitude of microscopic roughness of the rest of the ice surface is less than the linear dimensions of a CCl_4 molecule, the state of CCl_4 adsorbate on the remaining microporous ice surface should be similar to the state of CCl_4 adsorbate on solid D_2O ice. These assumptions are in perfect agreement with the CCl_4 TPD spectra obtained at various CCl_4 exposures. Figure 13 illustrates the state of the CCl_4 adsorbate and the desorption pathways at various CCl_4 coverages.

At CCl_4 exposures below 0.75×10^{-5} Torr s (Figure 13a), the condition $\eta < \eta_{cr}$ is satisfied. Small CCl_4 clusters formed in the pores are easily buried in the near surface region of the ice film as the micropores collapse during TPD. The collapse of the micropores, driven by surface diffusion, occurs in the temperature range 110−130 K.[19,20] Desorption of CCl_4 clusters, however, is slow at these temperatures. A low desorption rate of CCl_4 clusters at these temperatures is consistent with collapse of the micropores and explains the efficiency of CCl_4 trapping as well as the absence of CCl_4 desorption features at 130−150 K at low CCl_4 coverages. The TPD spectra, thus, consist solely of δ- and ϵ-CCl_4 desorption features.

An increase in the CCl_4 exposure from 0.75×10^{-5} to 2×10^{-5} Torr s results in the growth of CCl_4 clusters inside the ice micropores (Figure 13b). As the mean cluster size increases, η is approaching η_{cr} and the δ- and ϵ-CCl_4 yields saturate. The σ-CCl_4 feature appears in the TPD spectra as the CCl_4 clusters become too large to be trapped during collapse of the micropores. The TPD spectra consist of δ-, ϵ-, and σ-CCl_4 peaks, with the α-CCl_4 peak in the vicinity of 145 K. A slight shift toward higher temperatures, observed in the position of the σ-CCl_4 peak, reflects the gradual growth in size of the CCl_4 clusters with CCl_4 exposure.

At CCl_4 exposures from 2×10^{-5} to 8×10^{-5} Torr s, an abrupt change is observed in σ-CCl_4 desorption. The σ-CCl_4 peak broadens and shifts to lower temperatures. This process is complete when the maximum of the σ-CCl_4 peak is located at 140 K. As the CCl_4 exposure increases, all of the micropores that can accommodate CCl_4 clusters are eventually filled. The adsorption of carbon tetrachloride proceeds through the forma-

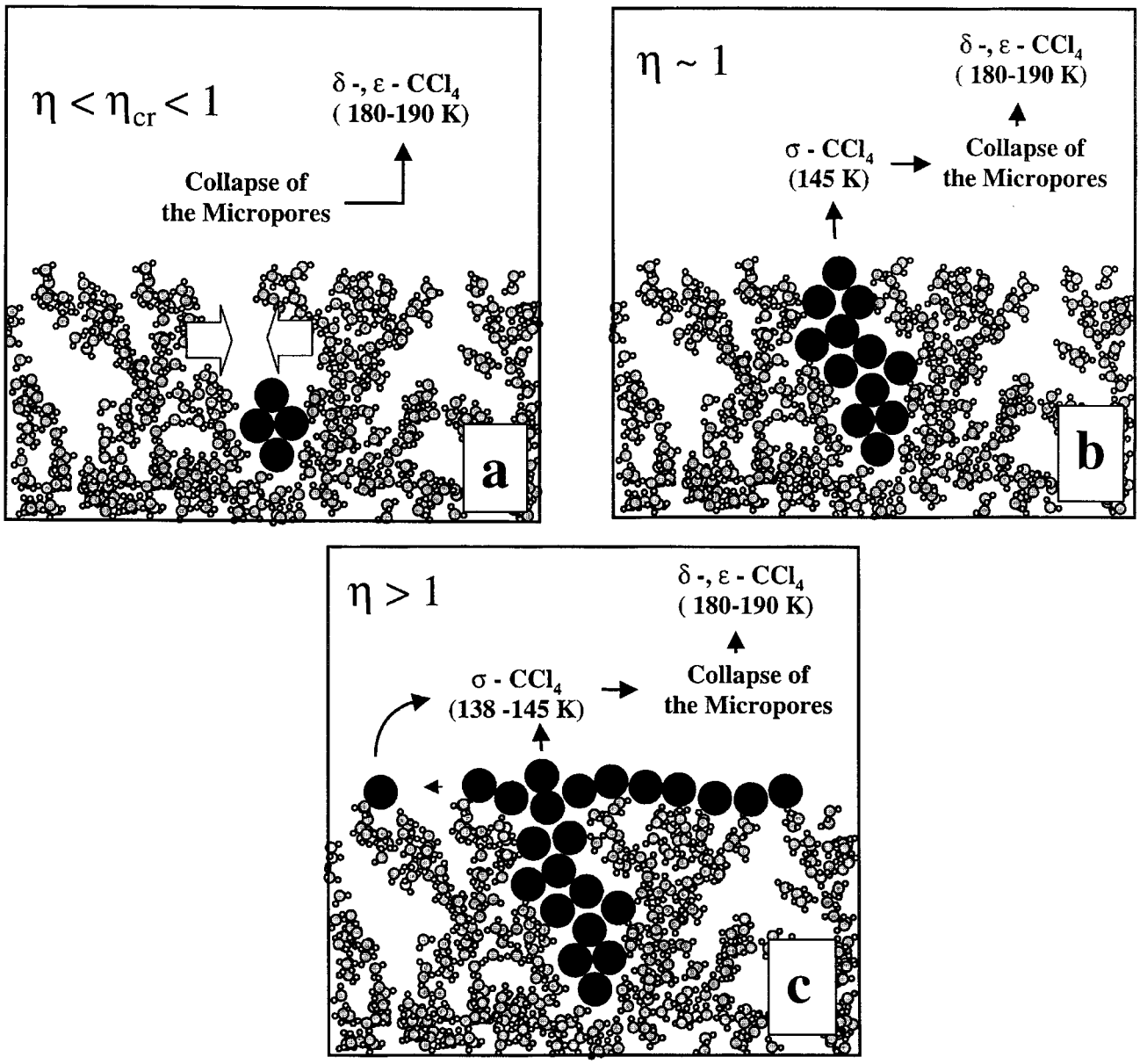

Figure 13. CCl_4 desorption form microporous amorphous ice at different CCl_4 coverages.

tion of two-dimensional islands on the rest of the ice surface (Figure 13 c). The σ-CCl_4 peak represents simultaneous desorption of the two-dimensional islands through the two-step mechanism described in the previous section, and the direct desorption of the three-dimensional clusters.

A closer look at the TPD spectra of CCl_4 from microporous D_2O ice obtained at a CCl_4 exposure of 4×10^{-5} Torr s reveals the dual nature of the σ-CCl_4 desorption feature. The shape and position of the σ-CCl_4 peak at this CCl_4 coverage can be approximated by a linear combination of the α-CCl_4 peak and the σ-CCl_4 peak obtained at some CCl_4 exposure, consistent with $\eta < 1$. Furthermore, σ-CCl_4 desorption from MA ice at an exposure of 8×10^{-5} Torr s is essentially identical to α-CCl_4 desorption in the TPD spectra of CCl_4 from SA ice. An Arrhenius plot of the TPD spectrum obtained at a CCl_4 exposure of 8×10^{-5} Torr s is shown in Figure 14. Similar to the α-CCl_4 plot, a linear dependence of the logarithm of the desorption rate on inverse temperature is clearly observed for the leading edges of the σ-CCl_4 desorption peaks. Arrhenius analysis results in an activation energy of 44 ± 1 kcal mol^{-1} for σ-CCl_4 desorption at the CCl_4 exposure of 8×10^{-5} Torr s. This value coincides with the activation energy for α-CCl_4 desorption from SA ice, demonstrating the validity of the above assumptions.

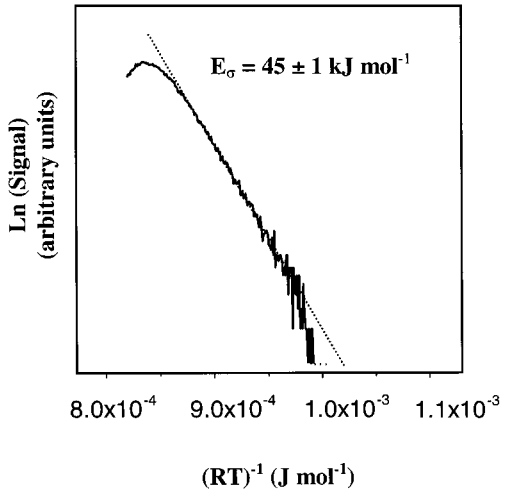

Figure 14. Arrhenius plot of the σ-CCl_4 peak in the case of a high CCl_4 exposure.

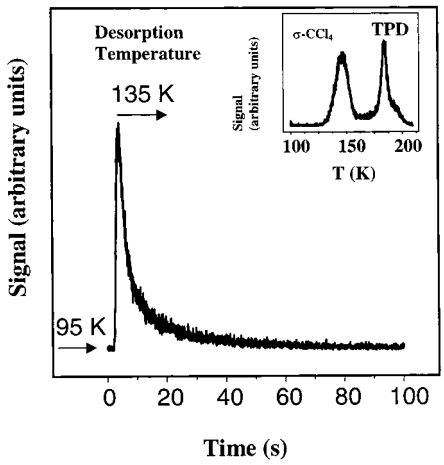

Figure 15. ID spectrum of CCl_4 in the case of low coverage. The TPD spectrum at identical CCl_4 exposure is shown for comparison.

The TPD spectra of CCl_4 from MA ice obtained at higher CCl_4 exposures can be interpreted in a manner analogous to CCl_4 desorption from SA ice. The only qualitative difference observed for CCl_4 desorption from the two types of amorphous ice at these exposures arises from the presence δ- and ϵ-CCl_4 desorption features in the TPD spectra of CCl_4 from MA ice.

It is interesting to compare the CCl_4 yield in 180−190 K temperature region to the total CCl_4 yield at high coverages. At a CCl_4 exposure of 8×10^{-5} Torr s, the CCl_4 coverage must be about a monolayer. Comparison of the δ- and ϵ-CCl_4 yields and the total CCl_4 yield at this exposure shows that only about 5% of all adsorbed CCl_4 molecules are trapped. This observation is in agreement with the assumption that only a small fraction of the MA ice surface is capable of trapping carbon tetrachloride.

Isothermal Desorption Spectra. To further demonstrate that adsorption of CCl_4 on MA ice at low exposures results in the formation of 3D clusters, we have briefly investigated isothermal desorption of CCl_4 obtained at exposures consistent with the condition $\eta \approx 1$. According to the argument derived in the previous section, at CCl_4 exposures of 2×10^{-5} Torr s most of the ice micropores accessible to CCl_4 molecules are filled, and the average size of the CCl_4 clusters reaches its maximum. The number of 2D islands at this critical exposure, however, should still be very low.

The ID and TPD spectra of CCl_4 obtained at exposures of 2×10^{-5} Torr s are shown in Figure 15. It can be argued that a rapid, monotonic signal decay observed in the ID spectrum is inconsistent with the proposed desorption mechanisms. If the CCl_4 trapping occurs abruptly after evaporating clusters reach some critical size, the ID spectra should demonstrate a rapid signal falloff at some desorption time. It should be noted, however, that such an ideal isothermal desorption behavior can only be expected if a number of unrealistic conditions are satisfied. First, collapse of the micropores and, thus, trapping of the CCl_4 clusters must be fast in comparison with CCl_4 cluster desorption. Second, the initial CCl_4 clusters must be approximately of the same size, i.e., the size distribution of the cluster ensemble must be narrow. Third, the collapse of ice micropores must be irreversible at the desorption temperature.

The complex dynamics of CCl_4 desorption as well as lack of a detailed knowledge of the MA ice surface morphology has deterred us from developing a simple quantitative model that would adequately describe the isothermal desorption kinetics. It is possible, however, to infer the activation energy of σ-CCl_4 desorption from the ID spectra obtained at various desorption temperatures. Analysis of the ID spectra shown in Figure 15 reveals that only about 2% of the CCl_4 molecules escape from the ice surface during initial ramping of the temperature from 95 to 135 K. The desorption rates, averaged over a short time interval after a preset desorption temperature has been achieved can, therefore, be directly used in order to estimate the activation energy for σ-CCl_4 desorption.

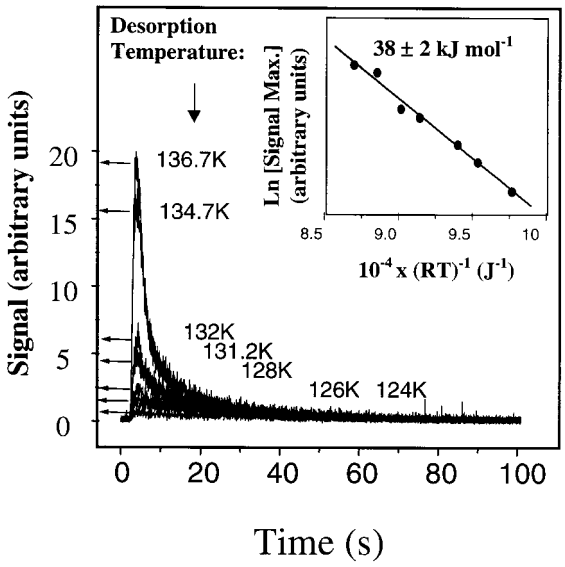

Figure 16. ID spectra of CCl_4 at various desorption temperatures, and the Arrhenius plot of the ID spectrum maxima.

ID spectra obtained for temperatures in the range 125−135 K and the Arrhenius plot of the ID spectra maxima are shown in Figure 16. The CCl_4 exposure was identical in all experiments (2×10^{-5} Torr s) and consistent with the condition $\eta \approx 1$. The apparent activation energy for σ-CCl_4 desorption (E_σ), determined from the slope of the Arrhenius plot, is 38 ± 2 kJ mol^{-1}. This value is in excellent agreement with the activation energy for sublimation of the condensed CCl_4 phase, supporting the conclusion that at low coverages, CCl_4 adsorbate is present on the microporous ice surface exclusively in the form of clusters.

Summary. TPD and ID experiments demonstrate that unlike adsorption on SA D_2O ice, CCl_4 adsorption on MA ice proceeds through formation of 3D CCl_4 clusters. At low coverages, CCl_4 clusters are easily trapped in the near-surface region of the ice film. Trapped CCl_4 is released at much higher temperatures, consistent with sublimation of the ice film. Only clusters of some critical size can be trapped. At high coverages, CCl_4 clusters evaporate freely until the trapping can occur. When most of the micropores are filled, CCl_4 adsorption on MA ice proceeds through formation of two-dimensional islands similar to the adsorption on SA ice.

III. Transition from Microporous to Solid Amorphous D_2O Ice and Release of Trapped CCl_4. *TPD Spectra of CCl_4 from Amorphous D_2O Ice Films Vapor-Deposited at Various Temperatures.* To gain insights into the ice structure and to further validate the proposed CCl_4 desorption mechanisms, we have compared the TPD spectra of CCl_4 from ice films grown at various temperatures. In all experiments, the CCl_4 deposition conditions (i.e., deposition temperature and exposure) were identical, while the D_2O deposition temperature (T_{D_2O}) was varied from 95 to 130 K.

The TPD spectra of CCl_4 from D_2O ice films deposited at five different temperatures are shown in Figure 17. As T_{D_2O} increases, a shift toward lower temperatures in the position of the σ-CCl_4 peak as well as an increase in the σ-CCl_4 yield are clearly observed. At elevated temperatures of D_2O deposition,

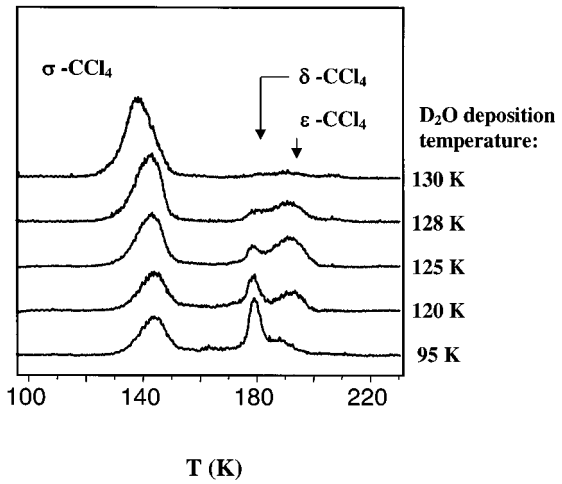

Figure 17. TPD spectra of CCl_4 from D_2O ice, deposited at various temperatures.

the microstructure of the resulting amorphous ice is characterized by reduced porosity and surface roughness. As the roughness of the ice surface decreases, the cluster formation is inhibited and two-dimensional CCl_4 islands become a dominating state of the CCl_4 adsorbate. These changes in the ice morphology are reflected in the gradual temperature shift of the σ-CCl_4 peak toward lower temperatures.

Though the net yield from the desorption of trapped CCl_4 is declining in the entire range of D_2O deposition temperatures, the δ- and ϵ-CCl_4 desorption features demonstrate rather complex dependence on the D_2O deposition temperature. The δ-CCl_4 yield declines gradually with T_{D_2O}. The ϵ-CCl_4 yield, however, first appears to grow, achieving a maximum value at T_{D_2O} of about 125 K, and only then rapidly declines. The δ- and ϵ-CCl_4 desorption features disappear completely from the CCl_4 TPD spectra at $T_{D_2O} \approx 130$ K.

Mechanism of δ-CCl_4 Desorption. It is clear from the bimodal character of the desorption feature in the 180−190 K temperature range that desorption of trapped carbon tetrachloride cannot be explained simply by a concurrent sublimation of D_2O and CCl_4. Smith et al. attributed the abrupt desorption of CCl_4 observed in TPD experiments with ultrathin CCl_4 films covered with an amorphous ice adlayer to formation of connected pathways in the overlaying ice during its transition from the amorphous to the crystalline form.[36]

We suggest that the δ-CCl_4 desorption occurs as a result of crystallization of the amorphous ice surrounding trapped CCl_4 clusters. Assuming that the density of the microporous amorphous ice is considerably lower than the density of crystalline ice, the mechanism of CCl_4 release during the phase transition can be easily understood. Trapped CCl_4 clusters are initially surrounded by amorphous ice that has a lower density than crystalline ice. At temperatures near 180 K, the spontaneous formation of crystallites occurs in the bulk and near the surface of the ice film. This process proceeds through the diffusion of D_2O molecules from the vicinity of a CCl_4 cluster to the nearest crystallites. The depletion of amorphous ice surrounding CCl_4 leads to formation of an escape path for trapped carbon tetrachloride.

It should be noted, however, that the temperature of δ-CCl_4 desorption is higher than the expected temperature of the phase transition from amorphous to crystalline D_2O ice.[13] This fact does not necessarily contradict the proposed mechanism of δ-CCl_4 desorption. Abrupt desorption of carbon tetrachloride is driven by the crystallization of the amorphous ice in the immediate vicinity of the CCl_4 clusters. It is reasonable to assume that the local crystallization kinetics are affected by hydrophobic interactions with trapped CCl_4 molecules. It has been demonstrated, for example, that interaction with a highly hydrophobic substrate may structurally influence a D_2O ice adlayer up to an average coverage of 50 monolayers.[44]

Mechanism of ϵ-CCl_4 Desorption. Finally, we would like to discuss the nature of the ϵ-CCl_4 desorption channel. The important characteristics of ϵ-CCl_4 desorption are summarized below.

First, ϵ-CCl_4 desorption occurs when δ-CCl_4 desorption is almost complete. Second, unlike the δ-CCl_4 desorption peak, the ϵ- CCl_4 desorption feature overlaps significantly with a D_2O TPD peak, indicating that ϵ-CCl_4 desorption and sublimation of the ice film occur simultaneously. Third, the ϵ-CCl_4 yield demonstrates complex dependence on D_2O deposition conditions. The ϵ-CCl_4 yield increases with D_2O deposition temperature, achieving a maximum at ∼125 K. On the basis of these observations, we would like to consider two probable mechanisms for ϵ-CCl_4 desorption.

It is possible that not all of the trapped CCl_4 molecules escape into the gas phase during the phase transition from amorphous to hexagonal crystalline ice. Residual CCl_4 is trapped at the grain boundaries in the bulk of the polycrystalline ice. Concurrent desorption of polycrystalline D_2O ice films and CCl_4 trapped at the grain boundaries results in the ϵ-CCl_4 desorption peak. This hypothesis, though consistent with the general characteristics of ϵ-CCl_4 desorption, fails to provide a simple explanation for the complex dependence of the ϵ-CCl_4 yield on D_2O deposition conditions. We, therefore, propose an alternative explanation based on the assumption that two coexisting types of microporous ice are formed in the near-surface region of ice films at the D_2O deposition temperatures used in these experiments.

Amorphous ice has been observed to coexist metastably with cubic crystalline ice (I_c) within certain temperature intervals.[45] The existence of the mixed amorphous/I_c ice provides a reasonable explanation of the observed TPD spectra. At temperatures in the range 110−130 K, the ice film growth is likely to proceed through formation of crystalline nuclei in the near-surface region of the ice films. We propose that the ϵ-CCl_4 desorption originates from CCl_4 trapped between the crystallites of the cubic ice. The differences in the temperature and the character of δ-CCl_4 and ϵ-CCl_4 desorption can be understood if the relative differences in densities of the two forms of ice are taken into consideration. Abrupt δ-CCl_4 desorption occurs through fractures or fissures created by stresses arising from density differences in the low-density amorphous ice and crystalline hexagonal ice. Since the density of cubic ice is close to the density of hexagonal ice, the phase transition to hexagonal ice, if such transition does take place at all on the time scale of TPD, must proceed without significant restructuring of the ice bulk and surface area. Desorption of CCl_4 initially trapped in cubic crystalline ice is likely to occur concurrently with sublimation of the D_2O ice film.

The observed dependence of the ϵ-CCl_4 yield on D_2O deposition condition is consistent with the proposed D_2O ice microstructure. D_2O vapor deposition at 95 K results in a highly porous structure, characterized by a large fraction of three-coordinated D_2O molecules. δ-CCl_4 desorption thus dominates at low temperatures of D_2O deposition. As the D_2O deposition temperature increases, growth of the crystalline ice nucleus occurs. At D_2O deposition temperatures from 95 to 125 K, the gradual increase in the ϵ-CCl_4 yield and the decline of the

δ-CCl_4 yield represent the gradual structural transition from amorphous to polycrystalline D_2O ice. We should emphasize that the overall effect of this transition is smoothing and solidification of the ice film, which follows from the fact that the sum of ϵ-CCl_4 and δ-CCl_4 yields is declining monotonically with D_2O deposition temperature. As the deposition temperature approaches 125 K, the amorphous ice vanishes completely. The rapid decline in the ϵ-CCl_4 yield in the temperature range from 125 to 130 K represents the formation of solid, pore-free, polycrystalline cubic ice.

Summary. The results presented in this section indicate that two coexisting forms of ice capable of trapping CCl_4 adsorbate are formed as a result of D_2O vapor deposition: (1) low-density amorphous D_2O ice; (2) higher density, cubic crystalline ice. δ-CCl_4 desorption is assigned to the abrupt release of carbon tetrachloride trapped in low-density amorphous D_2O ice upon its crystallization near 180 K. ϵ-CCl_4 desorption, concurrent with ice film sublimation, is attributed to desorption of carbon tetrachloride initially trapped in cubic ice.

Concluding Remarks

There are two significant aspects to the conclusions drawn from these experiments. First, the ability of D_2O ice vapor-deposited at cryogenic temperatures to trap molecules as large as CCl_4 implies a high porosity and microscopic surface roughness. Increasing the temperature of the ice deposition apparently reduces this trapping ability. These observations further validate the conclusions derived on the bases of spectroscopic measurements, that the morphology of ice films vapor-deposited at cryogenic temperatures depends dramatically on the ice deposition conditions; a low temperature and a high deposition flux apparently result in higher porosity and higher surface roughness of the amorphous ice. Second, we demonstrate that CCl_4 desorption kinetics at low coverages are extremely sensitive to the ice morphology. Therefore, desorption and trapping of CCl_4 can be utilized as a mass spectroscopic probe of the ice structure at the microscopic level. Since the CCl_4 adsorption in our experiments takes place after ice film deposition is complete, the comparison of CCl_4 TPD spectra from ice films grown under various conditions can be directly used to infer the changes in the ice structure.

Note Added after ASAP Posting

This article was released ASAP on 2/29/00 with an incorrect version of Figure 1. The correct version of Figure 1 now appears. The correct version was posted 3/2/00.

References and Notes

(1) Isakson, J. I.; Sitz, G. O. *J. Phys. Chem.* **1999**, *103*, 2044.
(2) Gotthold, M. P.; Sitz, G. O. *J. Phys. Chem.* **1998,** *102*, 9557.
(3) Schaff, Jason, E.; Roberts, Jeffrey, T. *Langmuir*. **1998**, *14*, 1478.
(4) Diehl, K.; Mitra, S. K.; Pruppacher, H. R. *Atmos. Res.* **1998,** *47*/*48*, 235.
(5) Chu, L. T.; Liang-Chu *J. Phys. Chem. B* **1997,** *101*, 6271.
(6) Banham, S. F.; Sodeau, J. R. J.; Horn, A. B.; McCoustra, M. R. S.; Chesters, M. A. *J. Vac. Sci. Technol.* **1996**, A *14* (3), 1620.
(7) Graham, J. D.; Roberts, J. T.; Anderson, L. D.; Grassian, V. H. *J. Phys. Chem.* **1996**, *100*, 19551.
(8) Banham, S. F.; Horn, A. B.; Koch, T. G.; Sodeau, J. R. *Faraday Discussions* **1995**, *100*, 321.
(9) Horn, A B.; Koch, T.; Chesters, M. A.; McCoustra, M. R. S.; Sodeau, J. R. *J. Phys. Chem.* **1994**, *98*, 946.
(10) Graham, J. D.; Roberts, J. T. *J. Phys. Chem.* **1994**, *98*, 5974.
(11) Horn, A. B.; Chester, M. A.; McCoustra, M. R. S.; Sodeau, J. R. *J. Chem. Soc. Faraday Trans.* **1992**, *88* (7), 1077.
(12) Hanson, D. R.; Ravishankara, A. R. *J. Phys. Chem.* **1992**, *96*, 2682.
(13) Eizenberg, D.; Kauzmann, W. *The structure and Properties of water*; Oxford University Press: New York, 1969.
(14) Hagen, W.; Tielens, A. G. G. M.; Greenberg, J. M.; *Chem. Phys.* **1981**, *56*, 367.
(15) Ghormley, J. A. *J. Chem. Phys.* **1967**, *46*, 1321.
(16) Adamson, A. W.; Dormant, L. M.; Orem, M. *J. Colloid Interface Sci.* **1967**, *25*, 206.
(17) Ocampo, J.; Klinger, J. *J. Colloid Interface Sci.* **1982**, *86*, 377.
(18) Pletzer, R.; Mayer, E. *Nature* **1986**, *319*, 298.
(19) Berland, B. S.; Brown, D. E.; Tolbert, M. A.; George, S. M. *Geophys. Res. Lett.* **1995**, *22*, 3493.
(20) Zondlo, M. A.; Onasch, T. B.; Warshawsky, M. S.; Tolbert, M. A.; Mallick, G.; Arentz, P.; Robinson, M. S. *J. Phys. Chem.* **1997**, *101*, 10887.
(21) Zhang, Q.; Buch, V. *J. Chem. Phys.* **1990**, *92*, 1512.
(22) Zhang, Q.; Buch, V. *J. Chem. Phys.* **1990**, *92*, 5004.
(23) Buch, V.; Devlin, J. P. *J. Chem. Phys.* **1991**, *94*, 4091.
(24) Rowland, B.; Devlin, J. P. *J. Phys. Chem.* **1993**, 97, 2485.
(25) Devlin, J. P. *J. Phys. Chem.* **1991**, 94, 812.
(26) Rowland, B.; Fisher, M.; Devlin, J. P. *J. Phys. Chem.* **1993**, 97, 2485.
(27) Rowland, B.; Fisher, M.; Devlin, J. P. *J. Chem. Phys.* **1995**, *95*, 1378.
(28) Devlin, J. P.; Buch, V. *J. Phys. Chem.* **1995**, 99, 16534.
(29) Stevenson, K. P.; Kimmel, G. A.; Dohnalek, Z.; Smith, R. S.; Kay B. D. *Science* **1999**, *283*, 1505.
(30) Gentry, W. R. *Atomic and Molecular Beam Methods*; Oxford: New York, 1988; Vol. 1.
(31) Daly, N. R. *Rev. Sci. Instrum.* **1960**, *31*, 264.
(32) Lofgren, P.; Ahlstrom, P.; Chakarov, D. V.; Lausmaa, J.; Kasemo, B. *Surf. Sci.* **1996**, *367*, L13.
(33) Chakarov, D. V.; Osterlund, L.; Kasemo, B. *Vacuum* **1995**, *46*, 1109.
(34) Brown, D. E.; George, S. M.; Huang, C.; Wong, E. K. L. Wong; Rider, K. B.; Smith, R. S.; Kay, B. D. *J. Phys. Chem.* **1996**, *100*, 4988.
(35) Schaff, J. E.; Roberts, J. T. *J. Phys. Chem.* **1996**, *100*, 14151 and our TPDMS experiments with multilayer D_2O films.
(36) Smith, R. S.; Huang, C.; Wong, E. K. L.; Kay, B. D. *Phys. Rev. Lett.* **1997**, 79 (5), 909.
(37) Blanchard, J. L.; Roberts, J. T. *Langmuir* **1994**, *10*, 3303.
(38) Nita, I.; Seki, S. *J. Chem. Soc. Jpn.* **1948**, *69*, 85.
(39) Asada, H.; Sekito, H. *Surf. Sci.* **1992**, *273*, 139.
(40) Ruiz-Suarez, J. C.; Vargas, M. C.; Goodman, F. O.; Scoles, G. *Surf. Sci.* **1991**, *243*, 219.
(41) Horn, A. B.; Chesters, M. A.; McCoustra, M. R. S.; Sodeau, J. R. *J. Chem. Soc., Faraday Trans.* **1992**, *88*, 1077.
(42) For a review, see: Bar-Nun, A.; Owen, T. *Astrophys. Space Sci. Libr.* **1998**, *227*, 353.
(43) Barabasi, A. L.; Stanley, H. E. *Fractal Concepts in Surface Growth*; Cambrige University Press: Cambrige, 1995.
(44) Engquist, I.; Lundstrom, I.; Liedberg, B.; Parikh, A. N.; Allara, D. L. *J. Phys. Chem.* **1997**, *106*, 33038.
(45) Jenniskens, P.; Blake, D. F. *Science* **1994**, *256*, 753.